Macromolecules

Article

pubs.acs.org/Macromolecules

# Construction of a Supramolecular Polymer by Bridged Bis(permethyl-β-cyclodextrin)s with Porphyrins and Its Highly Efficient Magnetic Resonance Imaging

Mo Sun, Heng-Yi Zhang, Bo-Wen Liu, and Yu Liu*

Department of Chemistry, State Key Laboratory of Elemento-Organic Chemistry, Nankai University, Tianjin 300071, P. R. China

Supporting Information

**ABSTRACT:** A supramolecular polymer is first constructed through the intermolecular inclusion complexation of bridged bis(permethyl-β-cyclodextrin) (**1**) with $Mn^{III}$-porphyrin bearing poly(ethylene glycol) (PEG) side chains ($Mn^{III}$-TPP) and characterized by UV/vis absorption spectroscopy, NMR, dynamic light scattering (DLS), atomic force microscopy (AFM), and transmission electron microscopy (TEM). $Mn^{III}$-TPP in the supramolecular polymer **1**·$Mn^{III}$-TPP would be reduced effectively to a higher electronic spins $Mn^{II}$-TPP by sodium ascorbate, but free $Mn^{III}$-TPP cannot be reduced in the same condition. The toxicity of the supramolecular polymer *in vitro* and the magnetic resonance imaging effectiveness both *in vitro* and *in vivo* are estimated, and the results obtained not only demonstrate the supramolecular polymer to have no cellular toxicity but also show the MR signal enhancement.

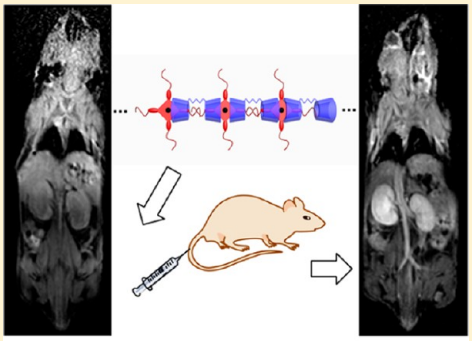

Supramolecular polymer as an MRI contrast agent



## INTRODUCTION

Supramolecular polymers, which are polymeric systems that extend beyond the molecule and utilize noncovalent interactions to direct their assembly, to control their conformations, and/or to define their behavior, have become a great interest and challenge in current scientific research.[1] Because of the nature of noncovalent interactions, supramolecular polymers show a variety of amazing properties, such as easy processability,[2] biocompatibility,[3] stimuli-responsiveness,[4] and self-healing.[5] Recently, Huang et al. have fabricated novel low-molecular-weight supramolecular gels utilizing reversible noncovalent interactions of crown ethers and ammonium salt.[6] Scherman et al. have reported the use of a series supramolecular polymers as supramolecular hydrogels which were considered important in biomedical and industrial applications. These supramolecular polymers were constructed simply by strong host−guest complexation with cucurbituril, naphthalene derivatives, and viologen-modified polymers.[7] With the aim of developing sophisticated highly ordered self-assembled structures from small building blocks by molecular recognition, self-replication, and self-organization based on noncovalent interactions, many researchers make a lot of efforts to design and fabricated functional supramolecular polymers in recent years.[8] However, the application of supramolecular polymers in diagnostic imaging of nanomedicine, especially using as an imaging agent, is still rare.

Successful, rapid, and precise diagnostic imaging of soft tissue has relied heavily on magnetic resonance imaging (MRI).[9,10] However, almost 50% of MRI examinations must need to use MRI contrast agents, which can improve the relatively low sensitivity of MRI and reduce the high cost and long acquisition time.[10−12] Paramagnetic gadolinium complexes are widely used as MRI contrast agents in clinical applications. The Food and Drug Administration (FDA) has restricted the use of these contrast agents because these contrast agents can induce patients with renal insufficiency to nephrogenic systemic fibrosis (NSF).[13]

$Mn^{II}$ is an essential metal element of cells and a cofactor for enzymes and receptors and has relatively high electronic spins (5/2), a long electronic relaxation time, and labile coordinated water molecule(s), which can make it act as an efficient MRI contrast agent.[14] Among Mn complexes, Mn porphyrins are good candidates as an imaging agent because they not only have the higher transmembrane permeability[15] than that of common $Mn^{II}$ chelates,[16] such as $Mn^{II}$ dipyridoxal diphosphate (Mn-DPDP, Teslascan)[17] and $Mn^{II}$ chloride (LumenHance),[18] but also have the less toxicity than that of MnO nanoparticles at a higher dose.[19] Nevertheless, $Mn^{II}$ inserted into the porphyrin ring can be quickly oxidized to $Mn^{III}$,[20] so its electronic spins also decrease correspondingly from 5/2 to 4/2. The character easy-oxidized limits the MRI efficiency of Mn porphyrins.[21]

It has been demonstrated that MRI contrast agents based on polymer/macromolecule platform can allow significant amplification by increasing the number of paramagnetic ions in the molecule[22] as well as decreasing the molecular rotation[23] and may have a substantial effect on tissue biodistribution and clearance.[24]

**Received:** April 19, 2013
**Revised:** May 22, 2013
**Published:** May 28, 2013

  

Cyclodextrins (CDs), nontoxic supramolecular hosts, gain more and more importance in polymer chemistry due to their ability to form noncovalent inclusion complexes with hydrophobic guest molecules, opening the opportunity to generate new supramolecular macromolecular architectures.[25] Bridged bis-CD possessing two CD cavities is an excellent monomeric unit to facilitate the construction of supramolecular polymers.[25c] Recently, we had constructed many CD-based supramolecular polymers by the noncovalent interaction of two cavities of bis-CD with 5,10,15,20-tetrakis(phenyl)-porphyrin (TPP),[26] and some of them exhibit amazing photophysical, photochemical, and electronic properties.[26b−e] And also, CD was found to stabilize the low-valent $Mn^{II}$-TPP in water, and the complex of CD and $Mn^{II}$-TPP was much more stable that of CD and $Mn^{III}$-TPP.[27]

Herein, we report the construction of a supramolecular polymer based on Mn-TPP and bridged bis(permethyl-$\beta$-CD), **1** (see Scheme 1), and this supramolecular polymer features noncytotoxic and efficient MRI enhancement properties. Considering the strong interaction of TPP with permethyl-$\beta$-CD reported by Kano's group,[28] bis(permethyl-$\beta$-CD) was used to benefit the formation of supramolecular polymers to increase the MRI capability. Furthermore, the cavity of CD can stabilize the low-valent $Mn^{II}$-TPP,[27] and this will help to prevent $Mn^{II}$-TPP oxidization so as to get a higher electronic spin. To increase stability and prolong blood circulation times, biocompatible poly(ethylene glycol) (PEG) was also introduced to Mn-TPP part,[29] which might promote the construction of supramolecular polymer due to its prohibition of the formation of a 1:1 complex of **1** and Mn-TPP.

**Scheme 1. Schematic Representation of Supramolecular Polymer 1·$Mn^{III}$-TPP**

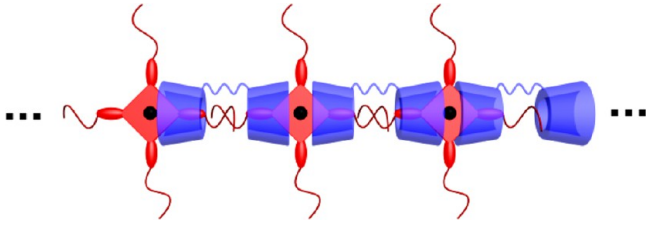

## RESULTS AND DISCUSSION

**Synthesis.** Bridged bis-CD **1** was obtained by 6-deoxy-6-isothiocyanatopermethyl-$\beta$-CD reacted with 1,2-ethanediamine, and mono-CD **2** was synthesized with methylamine with satisfactory yields. The products obtained were characterized by $^1$H NMR, $^{13}$C NMR, and HRMS. Porphyrins was synthesized according to ref 30 and then reacted with $Mn(OAc)_2$ in anhydrous methanol to afford $Mn^{III}$-TPP in 83% yield. The peaks belonging to the protons of TPP at $\delta = -2.77$ ppm in $^1$H NMR disappeared, demonstrating that Mn inserted into the porphyrin ring (Figures S9 and S12 in the Supporting Information). The supramolecular polymer was constructed by the complexation of Mn-TPP with **1** in aqueous solution. A control supramolecular complex was also synthesized by the complexation of Mn-TPP with **2**.

**UV/vis and NMR Spectra of $Mn^{III}$-TPP in the Presence and Absence of 1 or 2.** Figure 2 shows the UV/vis spectral changes of $Mn^{III}$-TPP upon addition of **1**. Its Soret band

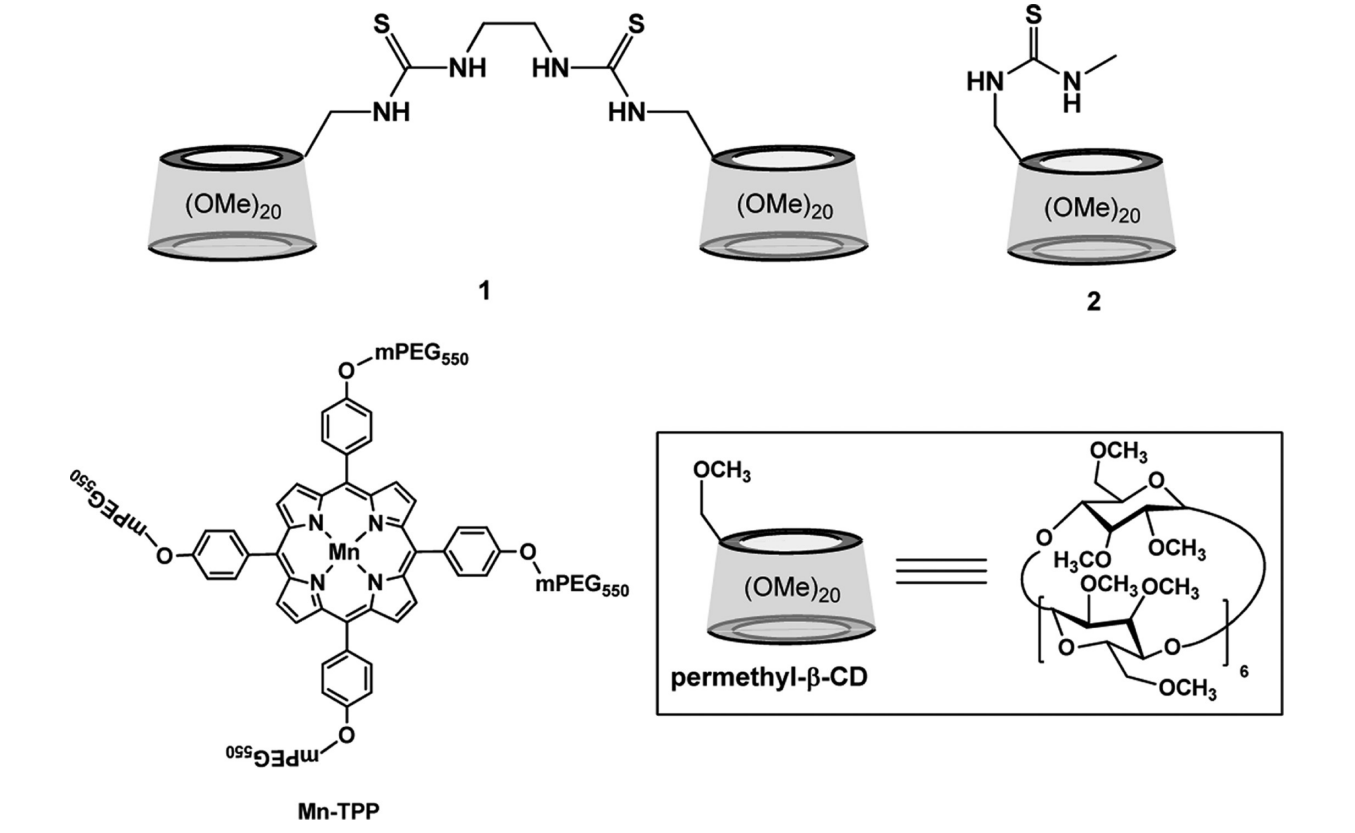


**Figure 1.** Structures of **1**, **2**, and Mn-TPP.


dx.doi.org/10.1021/ma400806s | Macromolecules 2013, 46, 4268−4275

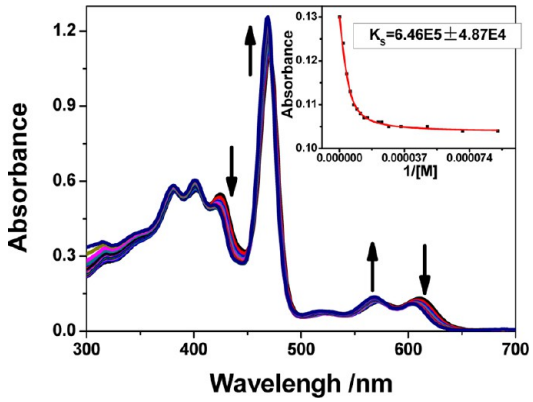


**Figure 2.** UV/vis spectral changes of $Mn^{III}$-TPP ($1.0 \times 10^{-5}$ M) in 0.1 M phosphate buffer at pH 7.4 upon addition of **1** at 25 °C. Inset: the curve-fitting results of **1**·$Mn^{III}$-TPP determined by using the nonlinear least-squares curve fitting.

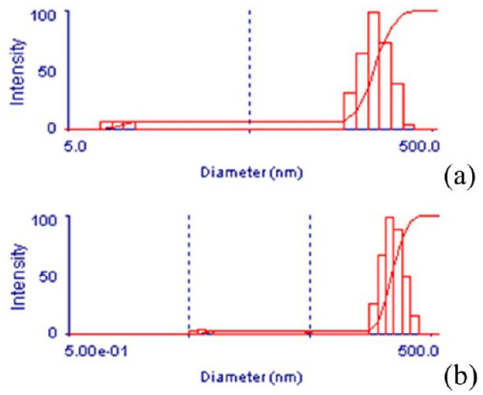


**Figure 3.** DLS for the supramolecular polymer (a) **1**·$Mn^{III}$-TPP and (b) **1**·$Mn^{II}$-TPP.

absorption at 466 nm gradually shifts to shorter wavelength with the increase of intensity, suggesting the formation of the complex between $Mn^{III}$-TPP and **1**. A similar phenomenon was also observed in the presence of **2** (Figure S13). Their host–guest binding stoichiometries were investigated using Job's plot method (Figures S14 and S15). For the complexation of $Mn^{III}$-TPP with **1**, the maximum value of $\Delta A$ (complex-induced changes of absorbance) appeared at a TPP molar fraction of 0.5, representing a 1:1 stoichiometry. For the complexation with **2**, this value appeared at 0.33, suggesting a 2:1 stoichiometry. Kano et al. first reported the extremely strong ability of permethyl-$\beta$-CD to include water-soluble porphyrins to afford trans-type 2:1 host–guest complexes.[28a] Our previous investigation also demonstrated that only the two CD at opposite positions intramolecularly include the TPP part.[26] The combination of the above stoichiometry and the previous results suggest that the complexation of $Mn^{III}$-TPP with **1** should form an *n*:*n* linear supramolecular polymer, while that with **2** should be a 1:2 complex. That is to say, the porphyrin entity acts as a bifunctional linker because of steric constraints between the threaded cylodextrin rings. Using a nonlinear least-squares method,[28b] the binding stability constant ($K_S$) values of $Mn^{III}$-TPP with **1** and **2** were determined. The $K_S$ value is $6.46 \times 10^5$ $M^{-1}$ for the complexation of $Mn^{III}$-TPP with **1**. There are two $K_S$ values for the complexation of $Mn^{III}$-TPP with **2**. That is, $K_{S1}$ equals $1.12 \times 10^5$ $M^{-1}$ and $K_{S2}$ is $5.85 \times 10^4$ $M^{-1}$.

NOESY spectral experiments of $Mn^{III}$-TPP in the presence of **1** and **2** in $D_2O$ were performed to confirm the interaction between host **1**/**2** and guest $Mn^{III}$-TPP. As shown in Figures S16 and S17, multiple cross-peaks regarding the protons of $\delta$ = 7.0–9.0 ppm assigned to the pyrrole protons with the protons of the secondary $OCH_3$ of PMCD were observed, indicating host–guest interactions existed.

**Size and Morphology of 1·$Mn^{III}$-TPP.** Dynamic laser scattering (DLS), atomic force microscopy (AFM), and transmission electron microscopy (TEM) were subsequently employed to identify the self-assembled size and morphology of the supramolecular complexes. DLS results showed that the complexation of **1** and $Mn^{III}$-TPP formed spectacular aggregates at a concentration of 0.05 mM with an average diameter of 202.7 nm (Figure 3a). In sharp contrast, neither **1**, $Mn^{III}$-TPP, nor complex **2**·$Mn^{III}$-TPP showed appreciable scattering intensity at the same concentration (Figures S18–S20), suggesting that no large-size aggregates were formed.

In the AFM image of the aggregate of **1** and $Mn^{III}$-TPP (Figure 4), a 1D linear morphology was found when mixing **1**

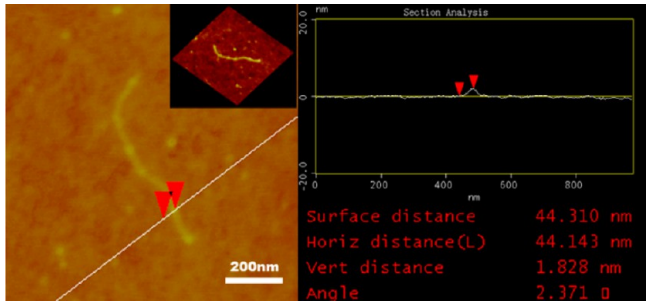


**Figure 4.** AFM image of supramolecular polymer **1**·$Mn^{III}$-TPP.

and $Mn^{III}$-TPP at equivalent molar ratio. The height of the aggregate was about 1.8 nm, representing the size of both **1** and $Mn^{III}$-TPP. The width appeared larger than its real size because of the broadening effect produced by the AFM tip.[31] Furthermore, the TEM images of the aggregate also showed a fine linear structure (Figures S21 and S22). Both TEM and AFM images confirmed that the aggregate **1**·$Mn^{III}$-TPP was linear supramolecular polymers. Meanwhile, the presence of Mn in the supramolecular polymer was confirmed by energy-dispersive analysis of X-rays (EDAX), as shown in Figure 5. The schematic representation of the supramolecular polymer **1**·$Mn^{III}$-TPP is illustrated in Scheme 1.

**Formation of Supramolecular Polymer 1·$Mn^{II}$-TPP.** In order to investigate the stability of $Mn^{II}$-TPP, the UV/vis spectral experiments of $Mn^{III}$-TPP and **1**·$Mn^{III}$-TPP in the presence and absence of excess sodium ascorbate were performed, respectively. The absorbance at 466 nm comes from Soret band of $Mn^{III}$-TPP, while that at 434 nm is ascribed to that in $Mn^{II}$-TPP.[27] As shown in Figure 6, the absorption spectrum of $Mn^{III}$-TPP hardly changed upon addition of sodium ascorbate, indicating that sodium ascorbate cannot reduce $Mn^{III}$ in TPP to $Mn^{II}$ at all. Comparing with that of $Mn^{III}$-TPP, no new bands appeared in the absorption of the supramolecular polymer **1**·$Mn^{III}$-TPP. Upon addition of sodium ascorbate, a new absorption band of **1**·$Mn^{III}$-TPP remarkably appeared at 434 nm accompanying the absorbance decrease at 466 nm. This observation indicated clearly that sodium ascorbate can reduce $Mn^{III}$ in **1**·$Mn^{III}$-TPP to $Mn^{II}$ effectively, and the cavity of CD plays a crucial role in stabilization of low-valent $Mn^{II}$-TPP. The similar results were obtained from the


dx.doi.org/10.1021/ma400806s | Macromolecules 2013, 46, 4268–4275

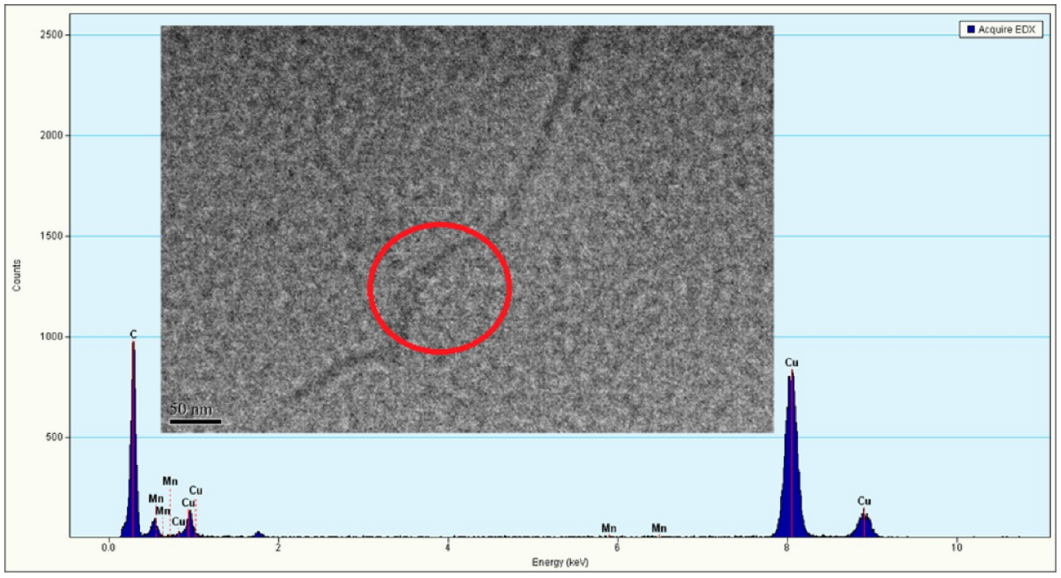


**Figure 5.** EDAX data measured by TEM mode. The data are collected from the region marked with a red circle. The scale bar is 50 nm.

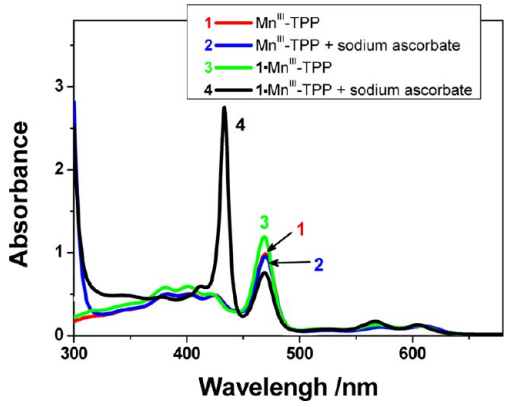


**Figure 6.** UV/vis spectra of $Mn^{III}$-TPP ($1.0 \times 10^{-5}$ M) and **1**·$Mn^{III}$-TPP ($1.0 \times 10^{-5}$ M) in the presence and absence of excess sodium ascorbate in 0.1 M phosphate buffer at pH 7.4 at 25 °C.

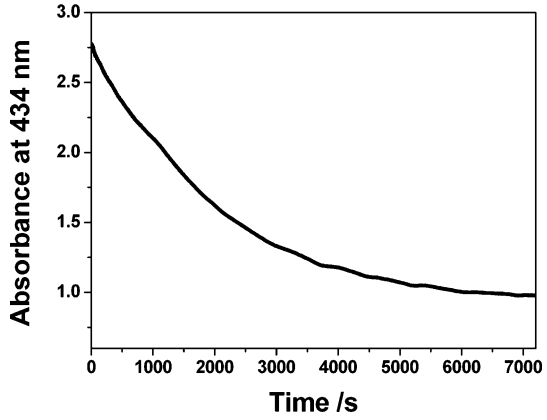


**Figure 7.** Time decay curve of the absorbance of **1**·$Mn^{II}$-TPP at 434 nm exposed in air.

UV/vis spectral experiments of **2**·$Mn^{III}$-TPP in the presence and absence of excess sodium ascorbate (Figure S23). DLS experiment of **1**·$Mn^{II}$-TPP gave a slightly bigger average diameter of 211.1 nm than the diameter of **1**·$Mn^{III}$-TPP (Figure 3b), suggesting that the valence states of Mn do not influence significantly on the size of the supramolecular polymer.

The stabilization of the supramolecular polymer **1**·$Mn^{II}$-TPP exposed in air was investigated subsequently because it could influence on the following *in vitro* and *in vivo* experiments. When **1**·$Mn^{II}$-TPP was exposed in air, the autoxidation of $Mn^{II}$-TPP to $Mn^{III}$-TPP occurred gradually (Figure 7). The half-life period was about 24 min in the open air according to the absorbance at 434 nm. Considering the MRI examination usually takes 30 min to accomplish and the content of dissolved oxygen in blood is lower than that in water, the stabilization of $Mn^{II}$-TPP by **1** was enough to use in clinic.

**Cellular Toxicity of Supramolecular Polymer 1·$Mn^{III}$-TPP.** To evaluate the cellular toxicity of the supramolecular polymer, the basic cell experiments were performed. NIH 3T3 cells (mouse embryonic fibroblast cells) were incubated with $MnCl_2$ ($5.0 \times 10^{-5}$ M), $Mn^{III}$-TPP ($5.0 \times 10^{-5}$ M), and **1**·$Mn^{III}$-TPP ($5.0 \times 10^{-5}$ M), and the number of living cells in each group was recorded from 24 to 72 h. As shown in Figures 8 and 9, the number of living cells in the supramolecular polymer **1**·$Mn^{III}$-TPP group was statistically equivalent to that in the blank group ($P > 0.05$) every day. The morphology of

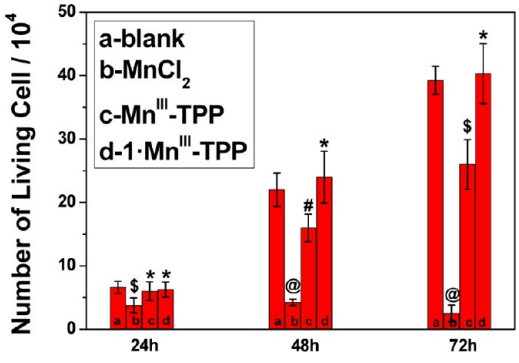


**Figure 8.** Number of living NIH3T3 cells in blank group and after treatment with unloaded $MnCl_2$, $Mn^{III}$-TPP, and **1**·$Mn^{III}$-TPP at different times: * indicate $P > 0.05$ versus blank group, $ indicate $P < 0.001$ versus blank group, @ indicate $P < 0.05$ versus blank group, and # indicates $P < 0.01$ versus blank group.


dx.doi.org/10.1021/ma400806s | *Macromolecules* 2013, 46, 4268−4275

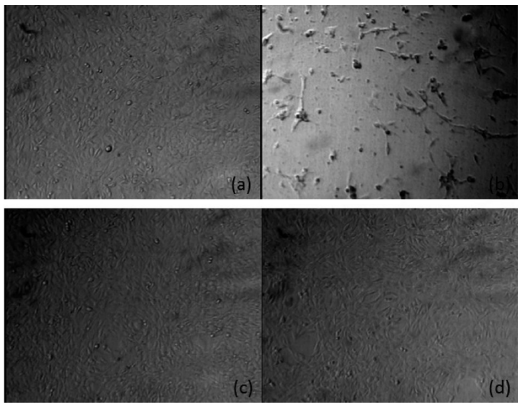


**Figure 9.** Images of living NIH3T3 cells in (a) blank group, (b) $MnCl_2$ group, (c) $Mn^{III}$-TPP group, and (d) **1**·$Mn^{III}$-TPP group after 72 h.

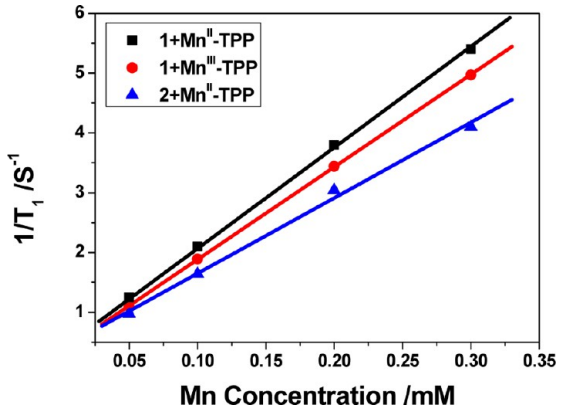


**Figure 11.** Relaxivity plots for **1**·$Mn^{II}$-TPP, **1**·$Mn^{III}$-TPP, and **2**·$Mn^{II}$-TPP.

living cells in the **1**·$Mn^{III}$-TPP group was also similar to that in the blank group. All these results suggested that the supramolecular polymer **1**·$Mn^{III}$-TPP was practically nontoxic. In the meanwhile, we also found that the number of living cells in the $Mn^{III}$-TPP group was little less than that in the blank group ($P < 0.01$) after 48 h, which indicated that $Mn^{III}$-TPP may had some influence on cell proliferation. The number of living cells in the $MnCl_2$ group was much less than that in the blank group ($P < 0.05$), and the morphology of living cells was notably different from that in the blank group. These observations imply $MnCl_2$, as one of the earliest contrast agents, may have some systemic toxicity.

**Relaxivities of Supramolecular Polymer 1·$Mn^{II}$-TPP.** To evaluate the *in vitro* efficiency of these agents, the longitudinal relaxivities $r_1$, which reflects the relaxation enhancement of solvent water protons in the presence of supramolecular assemblies in water at a concentration of 1 mM, were obtained with the aid of a 3 T MRI systems utilizing a standard, inversion–recovery sequence at room temperature. Relaxivity values $r_1$ were calculated through the curve fitting of $1/T_1$ relaxation time ($s^{-1}$) versus the Mn concentration (mM).

$$1/T_{1,\mathrm{obs}} = 1/T_{1,\mathrm{dw}} + r_1[\mathrm{M}]$$

measured $^1$H relaxation time in the presence of supramolecular assemblies, $T_{1,\mathrm{obs}}$; water diamagnetic constant, $T_{1,\mathrm{dw}}$; and Mn concentration, [M].[32]

According to Figures 10 and 11, the supramolecular polymer **1**·$Mn^{II}$-TPP was found to have longitudinal relaxivity ($r_1$) of 16.72 $mM^{-1}$ $s^{-1}$, whereas the $r_1$ values of **1**·$Mn^{III}$-TPP and **2**·$Mn^{II}$-TPP were found to be 15.69 and 12.64 $mM^{-1}$ $s^{-1}$, respectively. The $r_1$ relaxivity for the supramolecular polymer **1**·$Mn^{II}$-TPP was much higher than the commercially available Gd contrast agents ($r_1 \approx 4$ $mM^{-1}$ $s^{-1}$). The $r_1$ value of **1**·$Mn^{II}$-TPP was about 30% more than that of **2**·$Mn^{II}$-TPP, which may be attributed to the higher molecular weights shorting the rotational correlation time of the whole molecule ($\tau_R$). Compared to the $r_1$ value of **1**·$Mn^{III}$-TPP, it was likely that only a marginal increase (about 7%) in the $r_1$ value of **1**·$Mn^{II}$-TPP was observed. Despite a larger spin number ($S = 5/2$) of **1**·$Mn^{II}$-TPP which provided that its electronic relaxation ($\tau_s$) is slow, the reason may be the internal flexibility of the supramolecular assembly.[33]

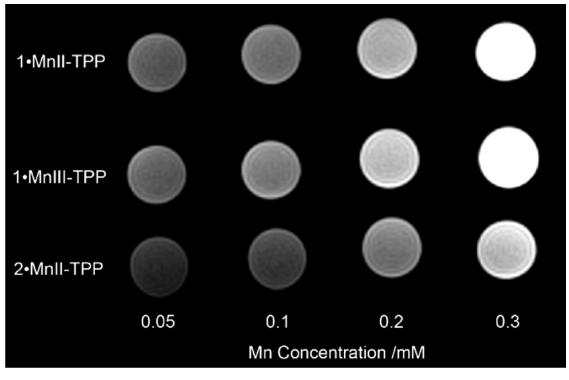


**Figure 10.** $T_1$-weighted images of **1**·$Mn^{II}$-TPP, **1**·$Mn^{III}$-TPP, and **2**·$Mn^{II}$-TPP.

***In Vivo* MR Imaging Test of Supramolecular Polymer 1·$Mn^{II}$-TPP.** In order to test the feasibility of the supramolecular polymer **1**·$Mn^{II}$-TPP as an MRI contrast agent, an *in vivo* MRI study was performed on mice. Contrast agent with a low dose is strongly desirable for *in vivo* MRI applications.[34] The effectiveness of the supramolecular polymer **1**·$Mn^{II}$-TPP as an MRI contrast agent was assessed *in vivo* using a 3 T clinical scanner. The results confirmed the strong $T_1$ effect to be seen in the *in vitro* studies. Figure 12 represents the time-dependent 2D coronal images of female athymic BALB/c nude mice before and after the injection of **1**·$Mn^{II}$-TPP at a dose of 0.03 mmol of Mn/kg. Strong contrast enhancement in blood was observed for the mice injected with **1**·$Mn^{II}$-TPP, indicating the fast circulation of supramolecular polymer in the bloodstream. Moreover, the MR signals in the urinary bladder and kidney of the mice injected with **1**·$Mn^{II}$-TPP were enhanced immediately after the injection of the contrast, implying excretion of the agents via renal filtration.[35] The mice injected with **1**·$Mn^{II}$-TPP displayed a very low signal enhancement in the liver at all time points, demonstrating that it would not accumulate in the liver and thus would not cause liver toxicity. More quantitative analysis data are shown in Figure 13. In the first 5 min, the contrast-to-noise ratios (CNRs) in blood, kidney, and bladder dramatically increased, revealing the rapid circulation of the supramolecular polymer within the bloodstream. Blood reached to the highest CNR at 5 min postinjection, while kidney at 10 min. Both blood and kidney maintained the maximum contrast enhancement performance up to at least 25 min. In contrast, the CNR of bladder organ continuously increased after the postinjection during the 25 min. By the way, the mice injected with **1**·$Mn^{II}$-TPP were alive after 36 h.


dx.doi.org/10.1021/ma400806s | *Macromolecules* 2013, 46, 4268–4275

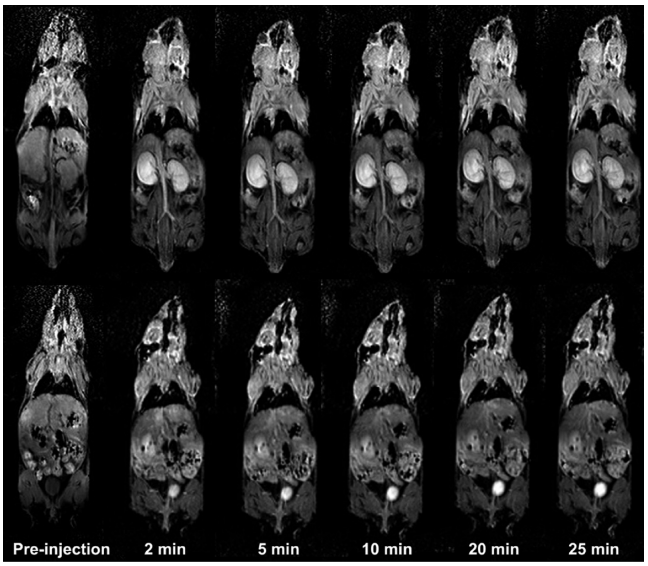


**Figure 12.** Representative 2D coronal $T_1$-weighted MR images of the mice at preinjection and 2, 5, 10, 20, and 25 min after intravenous injection of **1**·$Mn^{II}$-TPP MRI contrast agents at 0.03 mmol of Mn/kg.

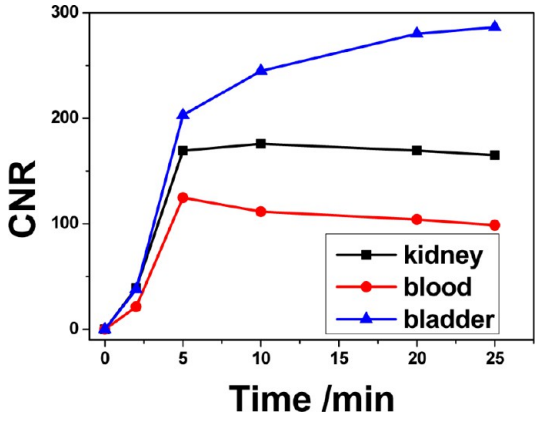


**Figure 13.** Contrast-to-noise ratio (CNR) in the blood, bladder, and kidney organs of mice at preinjection and 2, 5, 10, 20, and 25 min after intravenous injection of **1**·$Mn^{II}$-TPP MRI contrast agents at 0.03 mmol of Mn/kg.

## EXPERIMENTAL SECTION

**General Methods and Materials.** All chemicals were commercially available unless noted otherwise. NMR spectra were performed on a Bruker AV400 spectrometer. Mass spectra were performed on a Varian 7.0T FTICR-MS (MALDI). UV/vis spectra were recorded in a quartz cell (light path 10 mm) on a Shimadzu UV-3600 spectrophotometer equipped with a PTC-348WI temperature controller.

**AFM Measurements.** A $1.0 \times 10^{-7}$ M of sample solution was dropped onto newly clipped mica and then dried in air. The samples were performed by using a Multimode Nanoscope-IIIa scanning probe microscope (Digital Instruments Co., Ltd.) in tapping mode in air at room temperature.

**TEM Experiments.** The sample for TEM measurements was prepared by dropping the solution onto a copper grid. The grid was then air-dried. The samples were examined by a high-resolution TEM (Tecnai $G^2$ F20 microscope, FEI) equipped with a CCD camera (Orius 832, Gatan) operating at an accelerating voltage of 200 kV. Energy-dispersive X-ray spectroscopy (EDS) measurements were collected on a FEI Tecnai $G^2$ F20 TEM operating at an acceleration voltage of 200 kV.

**DLS Measurements.** The sample solution for DLS measurements was prepared by filtering solution through a 450 nm Millipore filter into a clean scintillation vial. The samples were examined on a laser light scattering spectrometer (BI-200SM) equipped with a digital correlator (Turbo Corr.) at 532 nm at a scattering angle of 90 °C.

**Cell Experiments.** Mouse embryonic fibroblast NIH 3T3 cells were seeded in a clear 24-well plate at a density of $2.25 \times 10^4$ cells/well in 800 μL of complete Dulbecco's Modified Eagle's Medium (DMEM) supplemented with 10% fetal bovine serum (FBS) and grown for 24 h at 37 °C in a humidified atmosphere of 5% of $CO_2$. NIH 3T3 cells were subsequently incubated with $MnCl_2$ ($5.0 \times 10^{-5}$ M), $Mn^{III}$-TPP ($5.0 \times 10^{-5}$ M), and **1**·$Mn^{III}$-TPP ($5.0 \times 10^{-5}$ M). After another 24, 48, and 72 h incubation, the number of living cells in every group was measured by using a cell-count assay. The number of living cells is expressed as the mean ± standard deviation, and $t$ = test was used for statistical analysis of the data. Differences were considered statistically significant when the $P$ value was less than 0.05.

**MRI and Relaxivity Measurements.** The supramolecular polymer **1**·$Mn^{II}$-TPP was obtained by adding excess sodium ascorbate into the supramolecular polymer **1**·$Mn^{III}$-TPP. The $T_1$-weighted images were acquired with a conventional spin-echo acquisition (repetition time, TR, 2000 ms) with echo time, TE, of 13 ms in a clinical 3.0 T magnetic resonance scanner (3 T Siemens Magnetom Trio). $T_1$ relaxivities were measured in a 3.0 T systems (3 T Siemens Magnetom Trio) at room temperature. Relaxivity values of $r_1$ were calculated through the curve fitting of $1/T_1$ relaxation time ($s^{-1}$) versus the Mn concentration (mM).

*In vivo* MR images were obtained by the following procedure. The *in vivo* experiments were approved by the Institutional Animal Care and Use Committee (IACUC) of Tsinghua University. Female BALB/c Nude mice (6 weeks, 14−16 g) were purchased from the Center of Biomedical Analysis of Tsinghua University. Before the imaging procedure and contrast agent administration, mice were anesthetized and kept under its influence for the duration of the experiment. MRI contrast agents were administered via a tail vein using 1.0 mL insulin syringes. The mice were placed in a human wrist coil and scanned in a Philips Achieva 3.0 T TX MRI scanner (Philips Healthcare, Best, The Netherlands) before and after injection using a fat suppression 3D FLASH sequence (TR = 7.8 ms, TE = 2.74 ms, 25 °C flip angle, 0.4 mm slice thickness, 128 × 256 × 48 matrix size, 50 × 100 × 24 $mm^3$ field of view, 0.39 × 0.39 × 0.5 $mm^3$ spatial resolution, 4 averages, 47.3 s acquisition time for one image set). The contrast-to-noise ratio (CNR) in a specific organ was calculated using the following equation: $CNR = (S_p - S_0)/\sigma_n$, where $S_p$ (postinjection) and $S_0$ (preinjection) denote the signal intensity in the region of interest (ROI) and $\sigma_n$ is the standard deviation of noise estimated from the background air.

**Preparation of 4.**[36] 6-Deoxy-6-azide-permethyl-β-CD (**3**) was prepared according to the literature procedures.[37] Under an argon atmosphere, a mixture of **3** (2.0 g, 1.4 mmol) and triphenylphosphine (4.0 g, 15.3 mmol) was dissolved in dichloromethane (20.0 mL). The solution was stirred overnight at room temperature. Then $CS_2$ (70.0 mL) was added to this mixture. The solution was stirred for another 24 h. Then the solvent was removed under reduced pressure. The residue was purified by silica gel column by using ethyl acetate to obtain compound **4** as a white solid (80%). $^1$H NMR (400 MHz, $CDCl_3$, $\delta$): 5.24−5.07 (m, 6H), 5.04 (d, $J$ = 3.7 Hz, 1H), 4.16 (d, $J$ = 12.9 Hz, 1H), 4.11−3.75 (m, 15H), 3.74−3.44 (m, 62H), 3.43−3.27 (m, 18H), 3.19 (m, 7H). HRMS (MALDI, $m/z$): $[M + Na]^+$ calcd for $C_{63}H_{109}NO_{34}SNa^+$, 1478.6444; found, 1478.6462.

**Preparation of 1.** To the solution of compound **4** (630.0 mg, 0.43 mmol) in acetonitrile (10.0 mL), 1,2-ethanediamine (13.0 mg, 14.5 μL, 0.22 mmol) was added under an argon atmosphere. The mixture was stirred overnight at room temperature. Then the solvent was removed under reduced pressure. The residue was purified by silica gel column by using chloroform−methanol (v/v = 30:1) to obtain compound **1** as a white solid (70%). $^1$H NMR (400 MHz, $CDCl_3$, $\delta$): 7.54 (s, 2H), 6.28 (s, 2H), 5.13 (d, $J$ = 10.4 Hz, 10H), 5.01 (s, 2H), 4.94 (s, 2H), 4.20−3.04 (m, 208H). $^{13}$C NMR (100 MHz, $CDCl_3$, $\delta$): 182.6, 99.9, 99.1, 99.0, 98.9, 82.3, 82.1, 81.9, 81.8, 81.6, 81.1, 80.4, 80.2, 80.1, 77.2, 71.7, 71.4, 71.0, 71.0, 71.0, 70.8, 70.0, 61.6, 61.5, 61.4,


dx.doi.org/10.1021/ma400806s | Macromolecules 2013, 46, 4268−4275

61.4, 61.3, 59.4, 59.2, 59.1, 59.0, 58.9, 58.7, 58.6, 58.5, 58.4, 43.9, 43.0. HRMS (MALDI, $m/z$): $[M + Na]^+$ calcd for $C_{128}H_{226}N_4O_{68}S_2Na^+$, 2994.3638; found, 2994.3680.

**Preparation of 2.** Under an argon atmosphere, a mixture of **4** (500.0 mg) and methanamine solution (40 wt % in $H_2O$) was stirred for 24 h. Then the solvent was removed under reduced pressure. The residue was purified by silica gel column by using chloroform−methanol (v/v = 40:1) to obtain compound **2** as a white solid (75%). $^1$H NMR (400 MHz, $CDCl_3$, $\delta$): 7.10 (s, 1H), 6.30 (s, 1H), 5.09 (dd, $J$ = 33.4, 17.3 Hz, 7H), 3.99−3.75 (m, 14H), 3.74−3.25 (m, 82H), 3.24−3.11 (m, 7H), 3.09 (d, $J$ = 2.8 Hz, 2H). $^{13}$C NMR (100 MHz, $CDCl_3$, $\delta$): 183.7 99.9, 99.8, 99.0, 99.0, 98.6, 82.4, 82.2, 82.1, 82.0, 81.9, 81.7, 81.6, 81.5, 81.3, 81.1, 80.5, 80.4, 80.3, 80.2, 72.8, 71.7, 71.4, 71.2, 71.1, 71.1, 70.9, 70.9, 70.8, 70.4, 61.6, 61.5, 61.4, 61.3, 59.4, 59.1, 59., 59.0, 59.0, 58.9, 58.7, 58.6, 58.6, 58.5, 58.4, 43.7, 32.2. HRMS (MALDI, $m/z$): $[M + Na]^+$ calcd for $C_{64}H_{114}N_2O_{34}SNa^+$, 1509.6866; found, 1509.6864.

**Preparation of $Mn^{III}$-TPP.** Under an argon atmosphere, a mixture of TPP[30] (200.0 mg) was dissolved in anhydrous methanol (50.0 mL) and stirred for 30 min. Then the solution of manganese acetate (200.0 mg) in anhydrous methanol (20.0 mL) was added to the above-mentioned mixture and refluxed for another 2 h. After being cooled, the solvent was reduced under vacuum. The residue was dissolved with $CH_2Cl_2$ and washed with brine twice. The organic phase was dried and evaporated off. The residue was purified by silica gel column by using $CH_2Cl_2$-methanol (v/v = 10:1) to obtain compound $Mn^{III}$-TPP as a greenish-black oil (83%).

## CONCLUSION

In summary, a supramolecular polymer was successfully fabricated through the intermolecular inclusion complexation of $Mn^{III}$-TPP with bridged bis(permethyl-$\beta$-CD), **1**, and it showed a great potential in bioimaging. The linear structure of the supramolecular polymer was confirmed by UV/vis spectra, NMR, DLS, AFM, and TEM analyses. UV/vis spectral experiments indicated that sodium ascorbate could reduce exclusively $Mn^{III}$-TPP to $Mn^{II}$-TPP in the supramolecular polymer, and the cavity of CD played a crucial role in stabilization of low-valent $Mn^{II}$-TPP. The cell experiments showed that the supramolecular polymer was practically nontoxic. *In vitro* MR imaging characterization exhibited considerably enhanced $T_1$ relaxivity for the supramolecular polymer compared to that for commercially available Gd contrast agent. Further *in vivo* MR imaging investigation in mice revealed prominently positive contrast enhancement of the supramolecular polymer within the blood, kidney, and urinary bladder of the mice. The research provides a new direction of the supramolecular polymer in bioimaging field.

## ASSOCIATED CONTENT

### Supporting Information

Characterization of compounds, HRMS, 2D NMR, UV/vis spectra, DLS, and TEM images. This material is available free of charge via the Internet at http://pubs.acs.org.

## AUTHOR INFORMATION

### Corresponding Author

*E-mail yuliu@nankai.edu.cn (Y.L.).

### Notes

The authors declare no competing financial interest.

## ACKNOWLEDGMENTS

We thank the 973 Program (2011CB932500) and the NNSFC (Nos. 20932004 and 91227107) for financial support.

## REFERENCES

(1) (a) Huang, F.; Scherman, O. A. *Chem. Soc. Rev.* **2012**, *41*, 5879−5880. (b) de Greef, T. F. A.; Meijer, E. W. *Nature* **2008**, *453*, 171−173. (c) Ciferri, A. *Supramolecular Polymers*; Taylor & Francis Group: Boca Raton, FL, 2005. (d) Brunsveld, L.; Folmer, B. J. B.; Meijer, E. W.; Sijbesma, R. P. *Chem. Rev.* **2001**, *101*, 4071−4097. (e) Guo, D.-S.; Liu, Y. *Chem. Soc. Rev.* **2012**, *41*, 5907−5921. (f) Harada, A.; Takashima, Y.; Yamaguchi, H. *Chem. Soc. Rev.* **2009**, *38*, 875−882.

(2) (a) Folmer, B. J. B.; Sijbesma, R. P.; Versteegen, R. M.; van der Rijt, J. A. J.; Meijer, E. W. *Adv. Mater.* **2000**, *12*, 874−878. (b) Niu, Z.; Huang, F.; Gibson, H. W. *J. Am. Chem. Soc.* **2011**, *133*, 2836−2839. (c) Park, T.; Zimmerman, S. C. *J. Am. Chem. Soc.* **2006**, *128*, 11582−11590.

(3) (a) Oohora, K.; Burazerovic, S.; Onoda, A.; Wilson, Y. M.; Ward, T. R.; Hayashi, T. *Angew. Chem., Int. Ed.* **2012**, *51*, 3818−3821. (b) Jin, H.; Huang, W.; Zhu, X.; Zhou, Y.; Yan, D. *Chem. Soc. Rev.* **2012**, *41*, 5986−5997. (c) Bastings, M. M. C.; de Greef, T. F. A.; van Dongen, J. L. J.; Merkx, M.; Meijer, E. W. *Chem. Sci.* **2010**, *1*, 79−88.

(4) (a) Yan, X.; Wang, F.; Zheng, B.; Huang, F. *Chem. Soc. Rev.* **2012**, *41*, 6042−6065. (b) Park, J. S.; Yoon, K. Y.; Kim, D. S.; Lynch, V. M.; Bielawski, C. W.; Johnston, K. P.; Sessler, J. L. *Proc. Natl. Acad. Sci. U. S. A.* **2011**, *108*, 20913−20917. (c) Xiao, T.; Feng, X.; Ye, S.; Guan, Y.; Li, S.-L.; Wang, Q.; Ji, Y.; Zhu, D.; Hu, X.; Lin, C.; Pan, Y.; Wang, L. *Macromolecules* **2012**, *45*, 9585−9594.

(5) (a) Hentschel, J.; Kushner, A. M.; Ziller, J.; Guan, Z. *Angew. Chem., Int. Ed.* **2012**, *51*, 10561−10565. (b) Fox, J.; Wie, J. J.; Greenland, B. W.; Burattini, S.; Hayes, W.; Colquhoun, H. M.; Mackay, M. E.; Rowan, S. J. *J. Am. Chem. Soc.* **2012**, *134*, 5362−5368. (c) Burnworth, M.; Tang, L.; Kumpfer, J. R.; Duncan, A. J.; Beyer, F. L.; Fiore, G. L.; Rowan, S. J.; Weder, C. *Nature* **2011**, *472*, 334−337. (6) Dong, S.; Zheng, B.; Xu, D.; Yan, X.; Zhang, M.; Huang, F. *Adv. Mater.* **2012**, *24*, 3191−3195.

(7) Appel, E. A.; Loh, X. J.; Jones, S. T.; Biedermann, F.; Dreiss, C. A.; Scherman, O. A. *J. Am. Chem. Soc.* **2012**, *134*, 11767−11773.

(8) Wojtecki, R. J.; Meador, M. A.; Rowan, S. J. *Nat. Mater.* **2011**, *10*, 14−27. (b) Aida, T.; Meijer, E. W.; Stupp, S. I. *Science* **2012**, *335*, 813−817. (c) Huang, Z.; Kang, S.-K.; Banno, M.; Yamaguchi, T.; Lee, D.; Seok, C.; Yashima, E.; Lee, M. *Science* **2012**, *337*, 1521−1526. (d) Pappalardo, A.; Ballistreri, F. P.; Destri, G. L.; Mineo, P. G.; Tomaselli, G.; Toscano, R. M.; Sfrazzetto, G. T. *Macromolecules* **2012**, *45*, 7549−7556.

(9) (a) Werner, E. J.; Datta, A.; Jocher, C. J.; Raymond, K. N. *Angew. Chem., Int. Ed.* **2008**, *47*, 8568−8580. (b) Lee, N.; Hyeon, T. *Chem. Soc. Rev.* **2012**, *41*, 2575−2589. (c) http://www.nobelprize.org/nobel_prizes/medicine/laureates/2003.

(10) (a) Lee, D. E.; Koo, H.; Sun, I. C.; Ryu, J. H.; Kim, K.; Kwon, I. C. *Chem. Soc. Rev.* **2012**, *41*, 2656−2672. (b) Na, H. B.; Hyeon, T. *J. Mater. Chem.* **2009**, *19*, 6267−6273. (c) Boros, E.; Polasek, M.; Zhang, Z.; Caravan, P. *J. Am. Chem. Soc.* **2012**, *134*, 19858−19868. (d) Garimella, P. D.; Datta, A.; Romanini, D. W.; Raymond, K. N.; Francis, M. B. *J. Am. Chem. Soc.* **2011**, *133*, 14704−14709. (e) Andolina, C. M.; Klemm, P. M.; Floyd, W. C., III; Fréchet, J. M. J.; Raymond, K. N. *Macromolecules* **2012**, *45*, 8982−8990.

(11) (a) Cheng, Z. L.; Thorek, D. L. J.; Tsourkas, A. *Angew. Chem., Int. Ed.* **2010**, *49*, 346−350. (b) Bellin, M. F. *Eur. J. Radiol.* **2006**, *60*, 314−323.

(12) Lauffer, R. B. *Chem. Rev.* **1987**, *87*, 901−927.

(13) (a) Pan, D. P. J.; Schmieder, A. H.; Wickline, S. A.; Lanza, G. M. *Tetrahedron* **2011**, *67*, 8431−8444. (b) Floyd, W. C.; Klemm, P. J.; Smiles, D. E.; Kohlgruber, A. C.; Pierre, V. C.; Mynar, J. L.; Fréchet, J. M. J.; Raymond, K. N. *J. Am. Chem. Soc.* **2011**, *133*, 2390−2393.

(14) (a) Tei, L.; Gugliotta, G.; Fekete, M.; Kalman, F. K.; Botta, M. *Dalton Trans.* **2011**, *40*, 2025−2032. (b) Kueny-Stotz, M.; Garofalo, A.; Felder-Flesch, D. *Eur. J. Inorg. Chem.* **2012**, 1987−2005.

(15) (a) Lee, T.; Zhang, X.-A.; Dhar, S.; Faas, H.; Lippard, S. J.; Jasanoff, A. *Chem. Biol.* **2010**, *17*, 665−673. (b) Aime, S.; Botta, M.; Gianolio, E.; Terreno, E. *Angew. Chem., Int. Ed.* **2000**, *39*, 747−750.

(16) Caravan, P.; Ellison, J. J.; McMurry, T. J.; Lauffer, R. B. *Chem. Rev.* **1999**, *99*, 2293−2352.

(17) Skjold, A.; Amundsen, B. H.; Wiseth, R.; Støylen, A.; Haraldseth, O.; Larsson, H. B.; Jynge, P. *J. Magn. Reson. Imaging* **2007**, *26*, 720−727.
(18) Small, W. C.; Macchi, D. D.; Parker, J. R.; Bernardino, M. E. *Acad. Radiol.* **1998**, *5*, S147−S150 discussion S156.
(19) Gilad, A. A.; Walczak, P.; McMahon, M. T.; Na, H. B.; Lee, J. H.; An, K.; Hyeon, T.; van Zij, P. C.; Bulte, J. W. *Magn. Reson. Med.* **2008**, *60*, 1−7.
(20) (a) Schwert, D. D.; Davies, J. A. *Top. Curr. Chem.* **2002**, *221*, 165−199. (b) Boucher, L. J. *Coord. Chem. Rev.* **1972**, *7*, 289−329.
(21) Drahoš, B.; Lukeš, I.; Tóth, É. *Eur. J. Inorg. Chem.* **2012**, 1975−1986.
(22) (a) León-Rodríguez, L. M. D.; Lubag, A.; Udugamasooriya, D. G.; Proneth, B.; Brekken, R. A.; Sun, X.; Kodadek, T.; Sherry, A. D. *J. Am. Chem. Soc.* **2010**, *132*, 12829−12831. (b) Courant, T.; Roullin, V. G.; Cadiou, C.; Callewaert, M.; Andry, M. C.; Portefaix, C.; Hoeffel, C.; de Goltstein, M. C.; Port, M.; Laurent, S.; Elst, L. V.; Muller, R.; Molinari, M.; Chuburu, F. *Angew. Chem., Int. Ed.* **2012**, *51*, 9119−9122.
(23) (a) Terreno, E.; Castelli, D. D.; Viale, A.; Aime, S. *Chem. Rev.* **2010**, *110*, 3019−3042. (b) Caravan, P. *Chem. Soc. Rev.* **2006**, *35*, 512−523. (c) Bryson, J. M.; Reineke, J. W.; Reineke, T. M. *Macromolecules* **2012**, *45*, 8939−8952.
(24) (a) Zhang, Z.; Kolodziej, A. K.; Greenfield, M. T.; Caravan, P. *Angew. Chem., Int. Ed.* **2011**, *50*, 2621−2624. (b) Liu, T.; Li, X.; Qian, Y.; Hu, X.; Liu, S. *Biomaterials* **2012**, *33*, 2521−2531. (c) Li, Y.; Qian, Y.; Liu, T.; Zhang, G.; Liu, S. *Biomacromolecules* **2012**, *13*, 3877−3886. (d) Li, X.; Qian, Y.; Liu, T.; Hu, X.; Zhang, G.; You, Y.; Liu, S. *Biomaterials* **2011**, *32*, 6595−6605. (e) Liu, T.; Qian, Y.; Hu, X.; Ge, Z.; You, Y.; Liu, S. *J. Mater. Chem.* **2012**, *22*, 5020−5030.
(25) (a) Chen, G.; Jiang, M. *Chem. Soc. Rev.* **2011**, *40*, 2254−2266. (b) Schmidt, B. V. K. J.; Hetzer, M.; Ritter, H.; Barner-Kowollik, C. *Macromolecules* **2013**, *46*, 1054−1065. (c) Liu, Y.; Chen, Y. *Acc. Chem. Res.* **2006**, *44*, 681−691.
(26) (a) Liu, Y.; Ke, C.-F.; Zhang, H.-Y.; Cui, J.; Ding, F. *J. Am. Chem. Soc.* **2008**, *130*, 600−605. (b) Zhang, Y.-M.; Chen, Y.; Yang, Y.; Liu, P.; Liu, Y. *Chem.—Eur. J.* **2009**, *15*, 11333−11340. (c) Gu, Z.-Y.; Guo, D.-S.; Sun, M.; Liu, Y. *J. Org. Chem.* **2010**, *75*, 3600−3607. (d) Zhang, Y.-M.; Chen, Y.; Zhuang, R.-J.; Liu, Y. *Photochem. Photobiol. Sci.* **2011**, *10*, 1393−1398. (e) Wang, K.-R.; Guo, D.-S.; Jiang, B.-P.; Liu, Y. *Chem. Commun.* **2012**, *48*, 3644−3646.
(27) (a) Kano, K.; Kitagishi, H.; Sone, Y.; Nakazawa, N.; Kodera, M. *Eur. J. Inorg. Chem.* **2006**, 4043−4053. (b) Goldberg, D. P.; Montalban, A. G.; White, A. J. P.; Williams, D. J.; Barrett, A. G. M.; Hoffman, B. M. *Inorg. Chem.* **1998**, *37*, 2873−2879.
(28) (a) Kano, K.; Tanaka, N.; Minamizono, H.; Kawakita, Y. *Chem. Lett.* **1996**, *25*, 925−926. (b) Kano, K.; Nishiyabu, R.; Asada, T.; Kuroda, Y. *J. Am. Chem. Soc.* **2002**, *124*, 9937−9944. (c) Kano, K.; Nishiyabu, R.; Yamazaki, T.; Yamazaki, I. *J. Am. Chem. Soc.* **2003**, *125*, 10625−10634. (d) Kano, K.; Nishiyabu, R.; Doi, R. *J. Org. Chem.* **2005**, *70*, 3667−3673. (e) Kano, K.; Kitagishi, H.; Tamura, S.; Yamada, A. *J. Am. Chem. Soc.* **2004**, *126*, 15202−15210. (f) Kano, K.; Kitagishi, H.; Kodera, M.; Hirota, S. *Angew. Chem., Int. Ed.* **2005**, *44*, 435−438.
(29) (a) Knop, K.; Hoogenboom, R.; Fischer, D.; Schubert, U. S. *Angew. Chem., Int. Ed.* **2010**, *49*, 6288−6308. (b) Villaraza, A. J. L.; Bumb, A.; Brechbiel, M. W. *Chem. Rev.* **2010**, *110*, 2921−2959.
(30) Long, J. W.; Kim, K.; Murray, R. W. *J. Am. Chem. Soc.* **1997**, *119*, 11510−11515.
(31) (a) Kirby, A. R.; Gunning, A. P.; Morris, V. J. *Biopolymers* **1996**, *38*, 355−366. (b) Rivetti, C.; Codeluppi, S. *Ultramicroscopy* **2001**, *87*, 55−66.
(32) Liao, Z.; Wang, H.; Wang, X.; Zhao, P.; Wang, S.; Su, W.; Chang, J. *Adv. Funct. Mater.* **2011**, *21*, 1179−1186.
(33) Tóth, E.; Helm, L.; Merbach, A. E. *Top. Curr. Chem.* **2002**, *221*, 61−101.
(34) Park, M.; Lee, N.; Choi, S. H.; An, K.; Yu, S.-H.; Kim, J. H.; Kwon, S.-H.; Kim, D.; Kim, H.; Baek, S.-I.; Ahn, T.-Y.; Park, O. K.; Son, J. S.; Sung, Y. N.; Kim, Y.-W.; Wang, Z.; Pinna, N.; Hyeon, T. *Chem. Mater.* **2011**, *23*, 3318−3324.
(35) (a) Tan, M.; Ye, Z.; Jeong, E.-K.; Wu, X.; Parker, D. L.; Lu, Z.-R. *Bioconjugate Chem.* **2011**, *22*, 931−937. (b) Mohs, A. M.; Zong, Y.; Guo, J.; Parker, D. L.; Lu, Z.-R. *Biomacromolecules* **2005**, *6*, 2305−2311.
(36) Haque, W.; Diakur, J. *J. Carbohydr. Chem.* **2001**, *20*, 17−29.
(37) (a) Hocquelet, C.; Blu, J.; Jankowski, C. K.; Arseneau, S.; Buisson, D.; Mauclaire, L. *Tetrahedron* **2006**, *62*, 11963−11971. (b) Reetz, M. T.; Waldvogel, S. R. *Angew. Chem., Int. Ed.* **1997**, *36*, 865−867.